Acknowledgements

We thank F. Briggs for the code used to predict the delays. This work was funded by the EU TMR network 'CERES'. The NRAO is a facility of the National Science Foundation operated under cooperative agreement by Associated Universities. The WSRT operated by ASTRON is supported by the Netherlands Organization for Scientific Research (NWO).

Competing interests statement

The authors declare that they have no competing financial interests.

Correspondence and requests for materials should be addressed to A.G.B. (e-mail: ger@astron.nl).

Mesoscopic superconductor as a ballistic quantum switch

A. S. Mel'nikov*† & V. M. Vinokur†

** Institute for Physics of Microstructures, Russian Academy of Sciences, 603950, Nizhny Novgorod, GSP-105, Russia*
† Argonne National Laboratory, Argonne, Illinois 60439, USA

Several key experiments[1–3] have revealed a rich variety of vortex structures in mesoscopic superconductors in which only a few quanta of magnetic flux are trapped: these structures are polygon-like vortex 'molecules' and multi-quanta giant vortices. Ginzburg–Landau calculations[4] confirmed second-order phase transitions between the giant vortex states and stable molecule-like configurations[5]. Here we study theoretically the electronic structure and the related phase-coherent transport properties of such mesoscopic superconductor systems. The quasiparticle excitations in the vortices form coherent quantum-mechanical states that offer the possibility of controlling the phase-coherent transport through the sample by changing the number of trapped flux quanta and their configuration. The sample conductance measured in the direction of the applied magnetic field is determined by the transparency of multi-vortex configurations, which form a set of quantum channels. The transmission coefficient for each channel is controlled by multiple Andreev reflections within the vortex cores and at the sample edge. These interference phenomena result in a stepwise behaviour of the conductance as a function of the applied magnetic field, and we propose to exploit this effect to realize a vortex-based quantum switch where the magnetic field plays the role of the gate voltage.

Giaever was the first to notice[6] that when magnetic flux gets trapped in a superconductor, the small normal areas that appear in parallel with superconducting areas influence transport characteristics. We find that phase-coherent transport mediated by the quasiparticle Andreev states associated with these normal domains enables us to tune the probability of tunnelling through a superconductor by changing the external magnetic field. We show that owing to a peculiar parity effect in the spatial distribution of the quasiparticle density of states (DOS), the ballistic conductance of a thin superconducting disk squeezed between very sharp contacts placed at the very centre of the disk (see Fig. 1) can alternate between finite and near-zero values as function of magnetic field. (The quasiparticle DOS has the form of a set of coaxial cylinders of finite radii, with an additional central spot if the number of trapped flux quanta is odd; the centre is hollow when the number is even.) In this regime, the mesoscopic superconductor realizes a quantum vortex switch where the external magnetic field plays the role of gate voltage.

We consider a thin disk of thickness $d < \lambda$ (where λ is the London penetration depth) and radius $R \ll \lambda_{\rm eff} = \lambda^2/d$. The structure of electronic states is determined by the interplay between the quasiparticle excitations bound within the cores of trapped vortices, which can either merge into multi-quanta vortices or form vortex molecules, and quasiparticle states bound near the disk edge. We start with the quasiparticle states of a giant vortex with a certain winding number m. In macroscopic samples, multi-quanta vortices are energetically unfavourable owing to the strong repulsion between the singly quantized vortices. But in mesoscopic samples, multi-quanta formations can be stable even at $H \ll H_{c2}$, because Meissner currents push vortices present in the sample close together. Here H_{c2} is the upper critical field. The winding number $m = 1$ corresponds to a conventional single vortex which carries a single flux quantum $\Phi_0 = \pi\hbar c/|e|$. Low-lying core quasiparticle states have been found[7], and can be viewed as the formation of standing quasiparticle waves owing to Andreev reflection of quasiparticles from the superconducting gap profile $\Delta(\mathbf{r})$ confining the vortex core: the quantitative theory of the quasiparticle states is based on the Bogolubov–de Gennes equations. In *s*-superconductors, the

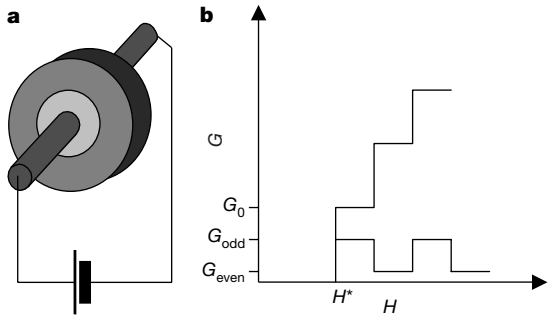

Figure 1 Phase-coherent transport through a few-flux-quanta superconductor. **a**, Mesoscopic superconducting disk placed between the two normal metal contacts; **b**, ballistic conductance of a mesoscopic disk versus magnetic field for large-area contacts (step-like growth of conductance) and point contacts with area less than the core radius (alternating behaviour of conductance). G_0 is a single vortex ballistic conductance for a large-area contact, G_{even} (G_{odd}) is a ballistic conductance for giant vortices with an even (odd) winding number measured by a small-area contacts positioned at the disk centre. H^* is the field of the first vortex entry.

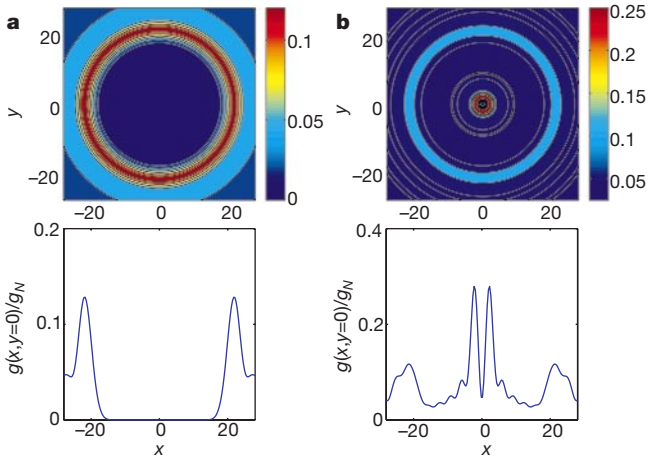

Figure 2 Spatial distribution of the thermodynamically averaged local DOS $g(\mathbf{r})$ normalized by its normal state value g_N for multi-quanta vortices. **a**, $m = 2$; **b**, $m = 3$. The x,y coordinates are measured in $1/k_F$, $T \approx \Delta/k_F\xi$; for $m = 2$, $k_F r_c = 20\sqrt{2}$; for $m = 3$, $k_F r_c = 40/\sqrt{3}$.

quasiparticle spectrum for small angular momentum quantum numbers μ is $\epsilon_\mu = \mu\Delta/|\mathbf{k}_\perp|\xi$ (ref. 7), where Δ is the superconducting gap far from the vortex axis, ξ is the coherence length, $|\mathbf{k}_\perp|$ is the absolute value of the wavevector in the plane perpendicular to the vortex, and μ is half an odd integer. This is the so-called anomalous branch of the quasiparticle energy, which, as function of μ, varies from $-\Delta$ to Δ, crossing zero as the impact parameter $b = \mu/|\mathbf{k}_\perp|$ of the particle in the core varies from $-\infty$ to ∞. For $m > 1$, the number of anomalous energy branches (per spin) crossing the Fermi level is equal to m (refs 8–10). If a vortex carries an odd number of flux quanta, one of these energy branches crosses the Fermi level at zero angular momentum $\mu = 0$ corresponding to $b = 0$ and, thus, the peak in the quasiparticle DOS at the vortex centre appears. A vortex with an even number m does not have such an energy branch, and the DOS peak at the vortex centre disappears. All anomalous branches in this latter case cross the Fermi level at finite impact parameter $b \approx r_c$, where r_c is the core radius. Making use of the quasiclassical approach, we obtain the quasiparticle energy spectrum as a function of the angular momentum quantum number μ and find the corresponding spatial distribution of the DOS $N(\epsilon, \mathbf{r})$. Shown in Fig. 2 is a thermodynamically averaged local DOS $g(\mathbf{r})$ normalized by its normal state value g_N, for $m = 2$ (Fig. 2a) and $m = 3$ (Fig. 2b):

$$g(\mathbf{r}) = \int_{-\infty}^{\infty} \frac{N(\epsilon, \mathbf{r})\mathrm{d}\epsilon}{4T\cosh^2(\epsilon/2T)} \qquad (1)$$

$g(\mathbf{r})$ is directly related to a zero-bias local tunnelling conductance between two reservoirs, and can be probed by scanning tunnelling spectroscopy[11].

Now we discuss DOS in the vortex molecule state. Treating splitting of a multi-quanta vortex into a small molecule with size $a \leq \xi$ as a perturbation, we observe that as soon as single-quanta vortices start to separate, each ring of the maximal DOS of a multi-quanta vortex breaks into m peaks. With an increase in the size of the molecule and, accordingly, in vortex spacing, some of the DOS peaks merge, and finally only m peaks at the centres of individual vortices survive. Typical spatial distributions of the corresponding thermodynamically averaged local DOS derived for two particular cases of $2\Phi_0$ and $3\Phi_0$ vortex molecules ($m = 2$ and $m = 3$) are shown in Fig. 3.

In the small samples with radius R comparable to the coherence length, the electronic structure is strongly affected by the edge electronic states. The finite magnetic field suppresses the order parameter near the disk edge, and creates a potential well for quasiparticles. Bound quasiparticle states form, owing to confinement by normal quasiparticle reflection at the disk edge and by Andreev reflection from the boundary of the classically impenetrable region. We derive the spectrum as a function of the angular momentum and magnetic field using the procedure analogous to that of refs 12, 13. Shown in Fig. 4 are the energy branches for a Meissner state ($m = 0$) as functions of dimensionless impact parameter $\tilde{b} = \mu/(k_\perp|R$. At $\mu \approx |k_\perp|R$ energy branches have minima, resulting in the sequence of discontinuities (step-like structure) in the energy and magnetic-field dependences of DOS. The appearance of a multi-quanta vortex at the disk centre gives rise to switching between the energy branches with different m: each subsequent flux quantum entering the disk reduces the depth of the edge potential well for quasiparticle excitations, and hence shifts the localized levels to higher energies. A further increase of the magnetic field increases the well depth (until the next flux quantum hops in). Therefore the DOS will show oscillations with the period $\delta H \approx \Phi_0/R^2$. The amplitude of oscillations increases with the decrease in the disk size, and is observable only in mesoscopic samples.

Now we turn to phase-coherent ballistic transport through the quasiparticle vortex states. Consider a mesoscopic superconducting disk squeezed between two contacts placed in the very centre of the disk (see Fig. 1: such contacts can be realized, for example, by STM tips pressed into disk surfaces). As the size of a few-fluxoid sample becomes less than the dephasing length, new physical processes come into play. Even in the case of a gapped quasiparticle spectrum and at the zero-temperature limit, single-particle ballistic transport through sufficiently thin disks can be mediated by quasiparticles with wavefunctions decaying in the current direction. Every flux quantum that enters the thin disk and joins either the vortex molecule or the multi-quanta giant vortex opens an additional channel for single-particle tunnelling. Thus the subsequent trapping of flux quanta results in a step-like increase in the disk conductance.

In a macroscopic superconducting system, the core states do not contribute to the electro-conductivity along the vortex lines, because the quasiparticle channels are shunted by the condensate: the normal current injected at the surface into the centre of the core converts to supercurrent over a certain length scale—which is less than the sample size. In the mesoscopic sample, the current does not have time to go outside the core, and one expects core states to dominate conductance. Yet the quasiparticle states still decay into the sample owing to multiple Andreev reflections from the boundaries of the vortex core. Our first step in the derivation of the quasiparticle conductivity is then the estimation of the decay length for each quasiparticle mode, and finding the corresponding fraction of the conducting channels contributing effectively to conductance. To this end, we look for the waveguide-like solution to the Bogolubov–de Gennes equations, and find the inverse decay length as:

$$\gamma_n \approx \frac{n\ln\Lambda}{k_\parallel \xi^2}, \qquad (2)$$

where n is an integer, $\Lambda \approx k_F\xi$, and $k_\parallel$ is the wavevector component

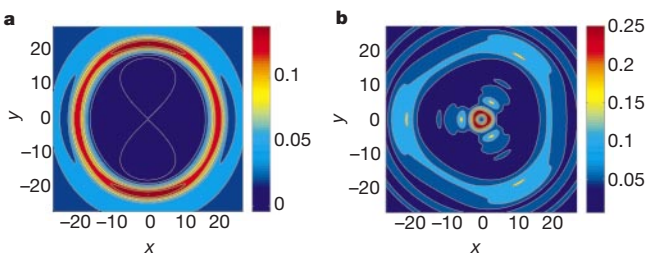

Figure 3 Spatial distribution of the thermodynamically averaged local DOS $g(\mathbf{r})$ for a vortex molecule. **a**, $m = 2$; **b**, $m = 3$. The x,y coordinates are measured in $1/k_F$, $T \approx \Delta/k_F\xi$. For $m = 2$, $k_F r_c = 20\sqrt{2}$; for $m = 3$, $k_F r_c = 40/\sqrt{3}$.

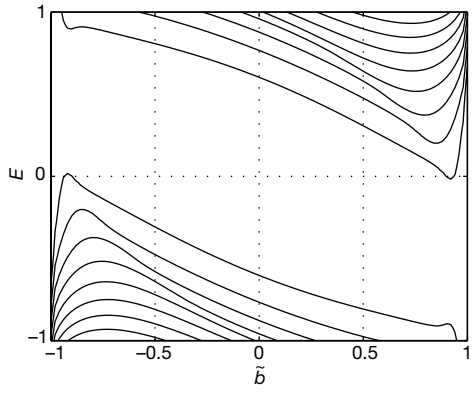

Figure 4 Energy spectrum for electronic states at the sample edge. Parameters used in these calculations are: $H = H^* = \phi_0/(\pi R\xi)$, $R = 15\xi$, $|\mathbf{k}_\perp|/k_F = 1$ (see text for details). $\tilde{b} = \mu/(|k_\perp|R)$ is the dimensionless impact parameter.

parallel to the vortex axis. k_F is the Fermi momentum. At small n, the decay length becomes much larger than the coherence length.

We now consider the ballistic conductance of the vortex of the length L. Consider the superconducting disk with the vortex as placed between the two normal metal reservoirs. Each quasiparticle mode contribution into the conductance is proportional to $(e^2/\hbar)\exp(-2\gamma_n L)$. Then the total conductance due to single-particle tunnelling processes becomes:

$$G \propto \frac{e^2}{\hbar} T_b \sum_{\mu} \sum_{n=n_{min}}^{n_{max}} \exp(-2\gamma_n L) \qquad (3)$$

where $n_{min} \approx \mu$, $n_{max} \approx k_F\xi$. We have assumed here the barrier transmission probability T_b to be the same for all channels (in a more detailed model, this coefficient should depend on the quantum numbers). In the case of interest we focus on, $\xi < L < k_F\xi^2$. Replacing sums over μ and n by the integrals, we arrive at the final estimate:

$$G \propto \frac{e^2}{\hbar} T_b (k_F\xi)^2 \frac{\xi^2}{L^2} \qquad (4)$$

For small samples of the size of several coherence lengths, single-particle conductance compares favourably with the two-particle Andreev contribution ($\propto T_b^2$). At large distances, $L > k_F\xi^2$, the $1/L^2$ power-law decay of the conductance crosses over to the exponential reduction $\propto \exp[-L/k_F\xi^2)]$, and in the long samples the single-particle current through the vortex channels is shunted by the supercurrent through the borders of the vortex core.

For the schematic experimental design shown in Fig. 1, we see that there is a notable dependence of the ballistic conductance behaviour on the magnetic field that exists at the area of the contact. For large-area contacts, all the additional channels—corresponding to new maxima of the DOS—that appear as flux quanta subsequently enter the disk, contributing to the conductivity. Hence such a 'large-contact-area device' will exhibit a step-like growth of conductance with increasing magnetic field (see Fig. 1). On the contrary, a point contact with an area much smaller than the area of the vortex core feels the density of states just at its location, and thus shows a strong dependence of the transmission probability T_b on μ and on contact position. Placing the point contact strictly at the centre of the disk, we observe either nearly zero (for even m, where the central spot in the DOS is absent) or finite alternating conductance for odd m, where single-particle tunnelling occurs via the central peak (see Fig. 1). This alternating conductance realizes a quantum switch, with magnetic field playing the role of gate voltage. Generally, the magnetic-field dependence of conductance will exhibit a mixture of the above step-like and alternating behaviours.

The ballistic contribution to the conductance dominates the quasiparticle transport at rather low temperatures, $T < \Delta\xi/L$; in all other cases, the conductance will be determined by the thermodynamically averaged DOS. Thus, experimental realization of ballistic quantum switch regime requires low temperatures—and pure, thin samples. □

Received 16 August; accepted 7 November 2001.

1. Boato, G. *et al.* Direct evidence for quantized flux threads in type II superconductors. *Solid State Commun.* **3,** 173–176 (1965).
2. McLachlan, D. S. Quantum oscillations and the order of the phase charge in a low k type II superconducting microcylinder. *Solid State Commun.* **8,** 1589–1593 (1970).
3. Geim, A. K. *et al.* Fine structure in magnetization of individual fluxoid states. *Phys. Rev. Lett.* **85,** 1528–1531 (2000).
4. Schweigert, V. A., Peeters, F. M. & Deo, P. S. Vortex phase diagram for mesoscopic superconducting disks. *Phys. Rev. Lett.* **81,** 2783–2786 (1998).
5. Chibotaru, L. F. *et al.* Symmetry-induced formation of antivortices in mesoscopic superconductors. *Nature* **408,** 833–835 (2000).
6. Giaever, I. in *Tunneling Phenomena in Solids* (eds Burstein, E. & Lundqvist, S.) 255–271 (Plenum, New York, 1969).
7. Caroli, C., de Gennes, P. G. & Matricon, J. Bound fermion states on a vortex line in a type II superconductor. *Phys. Lett.* **9,** 307–309 (1964).
8. Volovik, G. E. Vortex motion in Fermi superfluids and the Callan-Harvey effect. *JETP Lett.* **57,** 244–246 (1993).
9. Tanaka, Y. *et al.* Energy spectrum of the quasiparticle in a quantum dot formed by a superconducting pair potential under a magnetic field. *Solid State Commun.* **85,** 321–326 (1993).
10. Virtanen, S. M. M. & Salomaa, M. M. Multiquantum vortices in superconductors: Electronic and scanning tunneling microscopy spectra. *Phys. Rev. B* **60,** 14581–14584 (1999).
11. Hess, H. F. *et al.* Scanning-tunneling-microscope observation of the Abrikosov flux lattice and the density of states near and inside a fluxoid. *Phys. Rev. Lett.* **62,** 214–217 (1989).
12. Pincus, P. Magnetic-field-induced surface states in a pure type-I superconductor. *Phys. Rev. B* **158,** 346–353 (1967).
13. Azbel', M. Ya. & Blank, A. Ya. Magnetic surface levels in superconductors. *JETP Lett.* **10,** 32–35 (1969).

Acknowledgements

We thank G. Crabtree, G. Karapetrov, A. Koshelev, V. Moshchalkov, D. A. Ryzhov, S. V. Sharov, I. A. Shereshevsky and I. D. Tokman for discussions. This work was supported by the US DOE Office of Science, a NATO Collaborative Linkage Grant, and by the Russian Foundation for Fundamental Research.

Correspondence and requests for materials should be addressed to V.M.V. (e-mail: vinokur@msd.anl.gov).

A robust DNA mechanical device controlled by hybridization topology

Hao Yan, Xiaoping Zhang, Zhiyong Shen & Nadrian C. Seeman

Department of Chemistry, New York University, New York, New York 10003, USA

Controlled mechanical movement in molecular-scale devices has been realized in a variety of systems—catenanes and rotaxanes[1–3], chiroptical molecular switches[4], molecular ratchets[5] and DNA[6]—by exploiting conformational changes triggered by changes in redox potential or temperature, reversible binding of small molecules or ions, or irradiation. The incorporation of such devices into arrays[7,8] could in principle lead to complex structural states suitable for nanorobotic applications, provided that individual devices can be addressed separately. But because the triggers commonly used tend to act equally on all the devices that are present, they will need to be localized very tightly. This could be readily achieved with devices that are controlled individually by separate and device-specific reagents. A trigger mechanism that allows such specific control is the reversible binding of DNA strands, thereby 'fuelling' conformational changes in a DNA machine[9]. Here we improve upon the initial prototype system that uses this mechanism but generates by-products[9], by demonstrating a robust sequence-dependent rotary DNA device operating in a four-step cycle. We show that DNA strands control and fuel our device cycle by inducing the interconversion between two robust topological motifs, paranemic crossover (PX) DNA[10,11] and its topoisomer JX_2 DNA, in which one strand end is rotated relative to the other by 180°. We expect that a wide range of analogous yet distinct rotary devices can be created by changing the control strands and the device sequences to which they bind.

PX DNA (Fig. 1a, left) is a four-stranded molecule in which two parallel double helices are joined by reciprocal exchange (crossing over) of strands at every point where the strands come together[10,11]. JX_2 (Fig. 1a, right) is a topoisomer of PX DNA that contains two adjacent sites where backbones juxtapose without crossing over. The colour coding of the strands and labels in Fig. 1 indicates that the top ends, A and B, are the same in both molecules, but the bottom ends, C and D, are rotated 180°. This rotation is the basis for the operation of the device. We have used strand replacement[9] to interconvert the PX and JX_2 motifs.